Observation of the Interference Effect in Vibrationally Resolved Electron Momentum Spectroscopy of H_2

Zhe Zhang, Xu Shan,* Tian Wang, Enliang Wang, and Xiangjun Chen†
Hefei National Laboratory for Physical Sciences at Microscale and Department of Modern Physics, University of Science and Technology of China, Hefei 230026, China
(Received 6 May 2012; revised manuscript received 10 June 2013; published 14 January 2014)

We report the first measurement on vibrationally resolved electron momentum spectroscopy of H_2 by using a high-resolution $(e, 2e)$ spectrometer. The vibrational-specific experimental momentum profiles have been obtained and shown to be in agreement with calculations of $(e, 2e)$ ionization cross sections taking into account the vibrational wave functions. Distinct deviations from Franck-Condon predictions have been observed in vibrational ratios of cross sections, which can readily be ascribed to the Young-type two-center interference. Unlike previous $(e, 2e)$ work, the present observation of an interference effect does not rely on the comparison with the one-center atomic cross section.

DOI: 10.1103/PhysRevLett.112.023204 PACS numbers: 34.80.Gs

Electron momentum spectroscopy (EMS), or binary $(e, 2e)$ spectroscopy, is an electron-impact ionization experiment near the Bethe ridge, whose cross section is directly linked to the square modulus of a single-electron wave function in momentum space [1–3]. This unique ability of "imaging" electron momentum distributions for individual orbitals has been attracting continuous interest during the last several decades [1–7]. For molecules, EMS measures transitions from neutral states to final ionic states that involve the electronic, vibrational, and rotational motions. However, because of the limited energy resolution (typically 1–2 eV), vibrational and rotational states are not resolved and they are treated as degenerate. As a result, the average over initial-state degeneracy and the sum over final-state degeneracy have been carried out so far in EMS. This implies the loss of information on the motion of nuclei accompanying the ionization transitions.

Since the year 2000, progress has been made on improving the sensitivity by several groups through developing angle and energy dispersive EMS spectrometers (AEDMC-EMS) [8–11]. This opens the door to some unexploited areas of EMS [5–7], e.g., the molecular frame $(e, 2e)$ experiments [5,6] and the observation of interference effects on momentum profiles [7]. Very recently, an AEDMC-EMS [11] employing asymmetric noncoplanar kinematics has been built in our laboratory, and an alluring energy resolution of 0.5–0.6 eV (in full width at half maximum) has been achieved by monochromizing the incident electron beam. This makes it possible to tentatively measure the vibrationally resolved EMS for simple diatomic molecules.

The H_2 molecule, as the simplest diatomic molecule, has only one occupied molecular orbital and only one vibrational mode; it was one of the earliest benchmark molecules to be studied by EMS [12,13]. In this article, we report the first EMS measurements on the ionization of H_2 with final vibrational states of H_2^+ partially resolved. The experimental momentum profiles (XMPs) are compared with calculations of $(e, 2e)$ triple differential cross sections (TDCSs), taking into account the vibrational wave functions. On the other hand, in recent years there has been considerable interest in observing Young-type interference effects in the ionization of diatomic molecules. Such interference effects, arising from the coherent emission from two indistinguishable atoms, lead to the energy- or angle-dependent oscillations in cross sections that can be detected in ionizations by heavy ions [14,15], photons [16,17], and electrons [18–21]. The interference effect in $(e, 2e)$ of H_2 was first predicted by theory [18] and then observed by experiments employing coplanar asymmetric kinematics [19–21]. The effect was revealed by the suppression or enhancement of the binary or recoil peaks as compared to helium at the same kinematics. In binary $(e, 2e)$ experiments, the interference effect (also referred to as bond oscillation) was first discussed in the 1980s [22] and clearly observed only recently in experiments of CF_4 [7]. However, both of these observations rely on the comparison with an effective one-center atomic cross section to uncover the interferences. A recent photoionization study has demonstrated that the ratios of vibrationally resolved spectra of diatomic molecules provide a more straightforward way to observe Young-type interference [17]. In the present work, the vibrational ratios of EMS cross sections are also drawn as a function of momentum. Distinct deviations from Franck-Condon (FC) predictions have been observed. Analysis based on a similar model used in Ref. [17] clearly shows that these deviations can be ascribed to the two-center interferences.

EMS is based on an $(e, 2e)$ experiment in which an electron from a target is cleanly knocked out by a high-energy incident electron, and the residual ion acts as a spectator. From energy and momentum conservation, the binding energy ε_f and the momentum $\boldsymbol{p}$ of the target electron are given by

$$\varepsilon_f = E_0 - E_a - E_b, \quad (1)$$

$$\boldsymbol{p} = \boldsymbol{p}_a + \boldsymbol{p}_b - \boldsymbol{p}_0, \quad (2)$$

where E_i $\boldsymbol{p}_i (i = 0, a, b)$ are kinetic energies and momenta of the incident and two outgoing electrons, respectively. The spectrometer employed in this work has been described in detail elsewhere [11]. Briefly, a monochromatized incident electron is accelerated to 2500 eV plus a binding energy of H_2 $1s\sigma_g$ orbital before impinging on the gas-phase H_2 injected from a nozzle. The scattered electron passes through a fast electron analyzer at polar angle $\theta_a = -14°$ and is detected by a two-dimensional position sensitive detector over a large range of both energies and azimuthal angles. The ejected electron outgoing along a polar angle $\theta_b = 76°$ enters into a slow electron analyzer and is detected by a one-dimensional position sensitive detector.

Figure 1(a) illustrates the ionization process involved in this work—vibronic transition from the $X^1\Sigma_g^+$ ground state of H_2 to the $^2\Sigma_g^+(1s\sigma_g)$ ground state of H_2^+. At room temperature, the ionization starts from the $\mu = 0$ vibrational ground state of the target to a certain vibrational state μ' of the ion. Figure 1(b) shows the ionization energy spectrum obtained by high-resolution photoelectron spectroscopy [23]. The vibrational states of H_2^+ are well resolved, and the relative intensities of individual vibrational peaks are proportional to the FC factors. The binding energy spectrum (BES) measured in this work is shown in Fig. 1(c). Although the energy resolution (0.6 eV) is still not enough to resolve individual vibrational states, the shape of the profile is remarkably asymmetric, which is obviously the FC profile arising from a series of vibrational excitations.

A least-squares fitting has been carried out by utilizing a set of Gaussian functions (GFs) for individual ionization transitions to different vibrational states of H_2^+ in the BES. The width of each GF is fixed at present EMS instrumental energy resolution (0.6 eV), and their positions refer to the exact energies of the corresponding vibrational peaks determined by high-resolution photoelectron spectroscopy [23]. Thirteen GFs are used to identify transitions to the first thirteen vibrational states with quantum number $\mu' = 0$–12, respectively, and one more function is used to fit the states with $\mu' > 12$. A least-squares fitting program employing a Monte Carlo algorithm [24] has been used that can effectively avoid the divergence in the fitting processes. Hence, the XMPs, which are the momentum-dependent EMS cross sections, can be extracted for individual vibrational states by plotting areas under the corresponding fitted peaks as a function of target electron momentum. The results are shown in Figs. 2(b)–(k). For $\mu' > 8$ only the summation is plotted in Fig. 2(k) due to the large uncertainty of data. Benefitting from simultaneous accumulation of data in two dimensions (both energy and angle), the reliability of the deconvoluted results for the peaks with space smaller than the energy resolution has

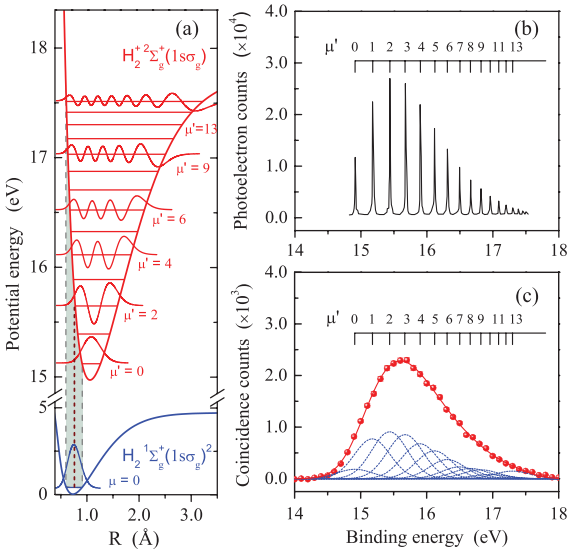

FIG. 1. (a) Vibronic transitions from the $X^1\Sigma_g^+$ ground state of H_2 to the $^2\Sigma_g^+(1s\sigma_g)$ ground state of H_2^+. The wave functions of some of the vibrational states are also shown. (b) The high-resolution photoelectron spectrum of H_2 [23]. (c) The BES of H_2 obtained in the present experiment. The dashed lines indicate the Gaussian peaks, and the solid line is the summed fit.

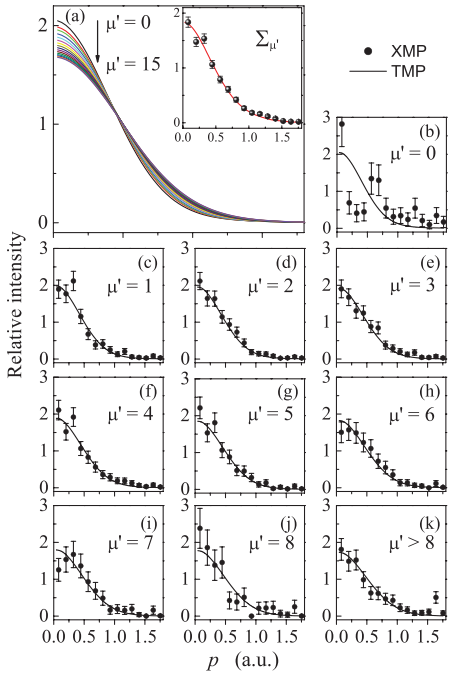

FIG. 2. (a) The TMPs for different H_2^+ vibrational states (shown by different colors). The inset shows the summed XMP for all vibrational states compared with the TMP calculated at equilibrium nuclear distance. The XMPs and corresponding TMPs for $\mu' = 0$–8 are shown in (b)–(j), respectively. The XMP and TMP presented in (k) are the sum of XMPs and TMPs for $\mu' > 8$. All profiles are area-normalized to unity.

been demonstrated to be favorably good in a wide range of experiments [25,26]. As can be seen from the figures, all the XMPs show the typical s-type character due to the ionization from $1s\sigma_g$ of H_2. Also included in the figures for comparison are the theoretical momentum profiles (TMPs). The calculation details are described as follows.

Within the binary encounter, as well as plane wave impulse approximations, the TDCS for $(e, 2e)$ ionization is [1]

$$\frac{d^3\sigma}{d\Omega_a d\Omega_b dE_b} = (2\pi)^4 \frac{p_a p_b}{p_0} f_{ee} |\langle \boldsymbol{p} I | G \rangle|^2. \quad (3)$$

Here f_{ee} is the electron-electron collision factor, which is essentially constant in EMS conditions, and $d\Omega$s are solid angles subtended by detectors. Therefore, the cross section is proportional to a structure term that is the square of the overlap between initial target state G and final ion state I. For molecules, G and I can be described in terms of the Born-Oppenheimer approximation as a product of separate electronic, vibrational, and rotational functions [1]:

$$|G\rangle = |0 V_\mu D_\nu\rangle, \quad (4)$$

$$|I\rangle = |i V'_{\mu'} D'_{\nu'}\rangle, \quad (5)$$

where V_μ and D_ν are the vibrational and rotational functions for the initial state. The indices μ and ν represent quantum numbers that specify the vibrational and rotational states, respectively. Final vibrational and rotational quantities are denoted by primes. The notations 0 and i represent the electronic states of the target and the ion. At room temperature the target is in its vibrational ground state $V_0(\mu = 0)$.

If the final vibrational states of the ion are distinguishable, while leaving the rotational states degenerate, the cross section reduces to

$$\frac{d^3\sigma}{d\Omega_a d\Omega_b dE_b} \propto \int \frac{d\Omega}{4\pi} |\langle \boldsymbol{p} V'_{\mu'} i | 0 V_0 \rangle|^2. \quad (6)$$

For H_2, which has only one vibrational mode, the structure amplitude $\langle \boldsymbol{p} V'_{\mu'} i | 0 V_0 \rangle$ can be simplified as [27]

$$\langle \boldsymbol{p} V'_{\mu'} i | 0 V_0 \rangle = \sqrt{\frac{1}{(2\pi)^3}} \int d\boldsymbol{\tau} d\boldsymbol{r} dR e^{-i\boldsymbol{p}\cdot\boldsymbol{r}} \times \phi_i^*(\boldsymbol{\tau}, R) X_{\mu'}^*(R) \phi_0(\boldsymbol{r}, \boldsymbol{\tau}, R) X_0(R) \quad (7)$$

where the electronic and vibrational wave functions of H_2 and H_2^+ are denoted as $\phi_0(\boldsymbol{r}, \boldsymbol{\tau}, R)$, $X_0(R)$ and $\phi_i(\boldsymbol{\tau}, R)$, $X_{\mu'}(R)$, respectively. The position vectors $\boldsymbol{r}$ and $\boldsymbol{\tau}$ are the coordinates of the knockout and residue electrons of H_2, while R is the internuclear distance.

For the close-shell configuration of the H_2 ground state, ignoring electron spin, the electronic wave function $\phi_0(\boldsymbol{r}, \boldsymbol{\tau}, R)$ can be described by the product of one-electron wave functions $\psi(\boldsymbol{r}, R)\psi(\boldsymbol{\tau}, R)$. The structure amplitude reduces to

$$\langle \boldsymbol{p} V'_{\mu'} i | 0 V_0 \rangle = \int dR X_{\mu'}^*(R) X_0(R) S^{(i)}(R) \varphi(\boldsymbol{p}, R) \quad (8)$$

where $S^{(i)}(R) = \int d\boldsymbol{\tau} \phi_i(\boldsymbol{\tau}, R) \psi(\boldsymbol{\tau}, R)$ is the overlap integral of the wave functions for the final ion and molecular residue left after the knockout of an electron from a molecular orbital, and $\varphi(\boldsymbol{p}, R) = (1/2\pi)^{3/2} \int d\boldsymbol{r} e^{-i\boldsymbol{r}\cdot\boldsymbol{p}} \psi(\boldsymbol{r}, R)$ is the Fourier transform of $\psi(\boldsymbol{r}, R)$.

From Eqs. (6) to (8) we can carry out stringent calculations of TDCS for the ionization transition from $\mu = 0$ of the H_2 $X^1\Sigma_g^+(1s\sigma_g)^2$ ground state to μ' of the H_2^+ $^2\Sigma_g^+(1s\sigma_g)$ ionic state. In the practical calculations, the vibrational wave functions are generated by numerically solving the vibrational Schrödinger equations for H_2 and H_2^+ by employing five-parameter Murrell-Sorbie potentials [28]. Figure 1(a) shows the resulting wave functions for the vibrational ground state of H_2 and vibrational states of H_2^+ together with their Murrell-Sorbie potential curves. The electronic wave functions for H_2 and H_2^+ are calculated at different internuclear distances R by the Hartree-Fock method with 6-311G basis sets using the GAUSSIAN 03 package [29].

The calculated TDCSs as a function of momentum, i.e., TMPs, for individual vibrational states of the ion with quantum number $\mu' = 0$–15 are shown in Fig. 2(a). For the sake of comparison, all the TMPs in Fig. 2(a) have been placed on a common intensity scale by area-normalizing to unity. It is also obvious that the shapes of all profiles are s-type. The differences between TMPs, however, are quite evident. Compared to the TMPs for high μ' states, the TMPs for low μ' states have larger intensities in the low momentum region and vice versa. In other words, the TMP becomes "fatter" as vibrational quantum number increases.

The TMPs are also plotted in Figs. 2(b)–(k) to compare with the corresponding XMPs. Here the TMPs are convoluted with instrumental momentum resolution of 0.10 a.u., and all the TMPs and XMPs in the figures are area-normalized to unity. The agreement in shape between experiments and theoretical calculations is fairly good. Although the experimental uncertainties are rather large, the general trend that XMP becomes fatter with an increase of vibrational quantum number is somehow observable. It is also interesting to look at the inset in Fig. 2(a), which shows the comparison between the summed XMP for all final vibrational states and the TMP of $1s\sigma_g$ calculated at equilibrium nuclear distance ($R_0 = 0.74$ Å). Good agreement has been achieved, confirming the widely accepted approximation for calculating TMPs of molecules at equilibrium nuclear geometries.

To highlight the differences, vibrational ratios of EMS cross sections are plotted in Fig. 3. We group the final vibrational states into three: the low quantum number group with $\mu' = 0$, 1, 2 denoted by capital letter L, the intermediate quantum number group with $\mu' = 4$, 5, 6 denoted by I and the high quantum number group with $\mu' = 9$–13 denoted by H. The theoretical EMS cross section $\sigma_{\mathrm{EMS}}(15)$ for $\mu' = 15$ is chosen as a reference, and the summed EMS cross sections of both experiments and theoretical calculations for these three groups are all divided by the reference $\sigma_{\mathrm{EMS}}(15)$. The experimental and theoretical results of $\sigma_{\mathrm{EMS}}(X)/\sigma_{\mathrm{EMS}}(15)$ $(X = L, I, H)$ are shown in Figs. 3(a)–(c) by solid circles and curves, respectively. Here, $\sigma_{\mathrm{EMS}}(X)$ are again area-normalized to unity for the convenience of comparison. Let us inspect Eq. (8) again. The estimations made by Levin *et al.* [27] for light diatomic molecules showed that the value $S^{(i)}(R)\varphi(\boldsymbol{p}, R)$ varies slowly in the range of nuclei coordinate R. So R can be chosen as equilibrium internuclear distance R_0, as an approximation. This actually implies the FC principle. Thus Eq. (8) reduces to

$$\langle \boldsymbol{p} V'_{\mu'} i | 0 V_0 \rangle = g_0^{\mu'} S^{(i)}(R_0)\varphi(\boldsymbol{p}, R_0) \tag{9}$$

where $g_0^{\mu'} = \int dR X^*_{\mu'}(R) X_0(R)$ is the FC factor. Within this approximation, the ratio of EMS cross sections for two final vibrational states $\sigma_{\mathrm{EMS}}(\mu'_1)/\sigma_{\mathrm{EMS}}(\mu'_2)$ will be equal to the quotient of the relevant FC factor $g_0^{\mu'_1}/g_0^{\mu'_2}$, which is a constant in the whole momentum range. However, one can see immediately from Figs. 3(a)–(c) that the observed ratios of $\sigma_{\mathrm{EMS}}(X)/\sigma_{\mathrm{EMS}}(15)$ $(X = L, I, H)$ obviously deviate from a constant (here it is unity due to the normalization), especially the low quantum number group L whose ratio declines sharply with the momentum. The stringent calculations based on Eq. (8) have reproduced the observations quite well. In photoionization of diatomic molecules, Canton *et al.* [17] also observed pronounced oscillations

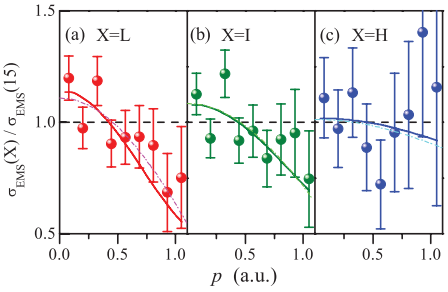

FIG. 3. The experimental and theoretical ratios of the EMS cross sections for different groups of vibrational states over the calculated cross section for $\mu' = 15$: (a) the low quantum number group $X = L$; (b) the intermediate quantum number group $X = I$; (c) the high quantum number group $X = H$. Solid circles and curves represent experimental and theoretical results. Dashed lines are Franck-Condon predictions. Chained lines are fitted curves of the model.

around a constant value predicted by FC approximations in their measured and calculated vibrational ratios of cross sections as functions of photon energy. They ascribed these deviations to the Young-type interference. Similar deviations from FC values in the present work can also be attributed to this. The interference effects in $(e, 2e)$ cross sections for randomly oriented homonuclear diatomic molecules could be modeled by multiplying a single atom cross section by an interference factor $1 + \sin(qR_0)/(qR_0)$ [18]. Here q is the magnitude of the recoil momentum of the residual ion, which is equal to p under the EMS condition. When taking into account vibrational states, following the method of Ref. [17], the vibrationally resolved cross section can be approximated by

$$\sigma_{\mathrm{EMS}}(\mu') = \sigma_0 \left| \int_0^\infty X_{\mu'}(R) \left[1 + \frac{\sin(pR)}{pR}\right]^{1/2} X_0(R) dR \right|^2 \tag{10}$$

where σ_0 is the equivalent one-center atomic cross section. By replacing the variable R in Eq. (10) by a characteristic value $R_{\mu'}$ associated with the μ' state, the vibrational ratio can further be approximated by

$$\frac{\sigma_{\mathrm{EMS}}(\mu_1')}{\sigma_{\mathrm{EMS}}(\mu_2')} = \frac{g_0^{\mu_1'}}{g_0^{\mu_2'}} \left[1 + \frac{\delta R_{\mu_1'}}{R_{\mu_2'}} \cos(pR_{\mu_2'})\right] \tag{11}$$

where $\delta R_{\mu'_1} = R_{\mu'_1} - R_{\mu'_2}$. This formula clearly predicts that the vibrational ratio should oscillate around the quotient of the FC factor. To evaluate the observations, the turning points on the potential curve for relevant vibrational states are adopted as the characteristic value $R_{\mu'}$, and the function $a_0[1 + a_1(\delta R_{\mu_1'}/R_{\mu_2'}) \cos(pR_{\mu_2'})]$ is employed to fit the vibrational ratios, where a_0 and a_1 are adjustable parameters. The turning point for the $\mu'_2 = 15$ state is 1.12 a.u., while the averaged values of turning points 1.6, 1.35, and 1.15 a.u. are used for $X = L$, I, H, respectively. The parameter a_1 is introduced to compensate for the approximations in the evaluations of $R_{\mu'}$ and thus is kept at the same value for all three fittings. The fitted curves are presented in Figs. 3(a)–(c) as chained lines. The agreement of the model fitting with the measured and calculated vibrational ratios signifies the Young two-center interference effect.

In summary, a vibrationally resolved EMS experiment on the H_2 molecule has been tentatively explored for the first time using a high-resolution $(e, 2e)$ spectrometer. The XMPs for ionization transitions to individual final vibrational states of the ion have been obtained by a deconvolution procedure and are compared with the stringent calculations of TDCSs, taking into account the vibrational wave functions. Good agreement has been achieved between measured and calculated vibrational-specific momentum profiles. The present work also demonstrates the Young-type interference effect in vibrationally resolved

TDCSs. The measured and calculated vibrational ratios of cross sections have revealed obvious deviations from FC values. Such deviations can readily be ascribed to the oscillation features in the vibrational ratios due to the two-center interferences. The vibrationally resolved experiment provides a more straightforward way to observe Young-type interference in electron impact ionization of diatomic molecules, since it does not rely on the comparison with a one-center atomic cross section. Moreover, if we look at individual XMPs again in Fig. 2, one may notice that the intensities at zero momentum show some probable oscillation feature with minima appearing at vibrational states $\mu' = 0$ and 7. There might be some interesting physics if this observation can be confirmed. Future efforts are expected be dedicated to achieve better energy resolution, higher statistics, and a wider momentum range of the instrument. In this way, we will be able to directly obtain the vibrational ratios between two experimental cross sections. It is essential for observing oscillations completely in the experiment, thereby removing any possible ambiguity related to the introduction of external parameters. Meanwhile, in order to include one whole period of oscillations within reach by experiment, the momentum range will be at least up to $2\pi/1.4$–4.5 a.u. for H_2. The latest version of EMS spectrometers [30,31], which have considerably higher sensitivity and a wider momentum range, would be desired.

This work was partially supported by the National Basic Research Program of China (Grant No. 2010CB923301) and the National Science Foundation of China (Grants No. 11327404, No. 20973160, No. 10904136, and No. 10979007).

*xshan@ustc.edu.cn
†xjun@ustc.edu.cn

[1] I. E. McCarthy and E. Weigold, Rep. Prog. Phys. **54**, 789 (1991).
[2] C. E. Brion, Int. J. Quantum Chem. **29**, 1397 (1986).
[3] M. A. Coplan, J. H. Moore, and J. P. Doering, Rev. Mod. Phys. **66**, 985 (1994).
[4] Y. Zheng, J. J. Neville, and C. E. Brion, Science **270**, 786 (1995).
[5] M. Takahashi, N. Watanabe, Y. Khajuria, Y. Udagawa, and J. H. D. Eland, Phys. Rev. Lett. **94**, 213202 (2005).
[6] S. Bellm, J. Lower, E. Weigold, and D. W. Mueller, Phys. Rev. Lett. **104**, 023202 (2010).
[7] N. Watanabe, X. J. Chen, and M. Takahashi, Phys. Rev. Lett. **108**, 173201 (2012).
[8] Y. Zheng *et al.*, J. Electron Spectrosc. Relat. Phenom. **112**, 67 (2000).
[9] M. Takahashi, T. Saito, M. Matsuo, and Y. Udagawa, Rev. Sci. Instrum. **73**, 2242 (2002).
[10] X. G. Ren, C. G. Ning, J. K. Deng, S. F. Zhang, G. L. Su, F. Huang, and G. Q. Li, Rev. Sci. Instrum. **76**, 063103 (2005).
[11] X. Shan, X. J. Chen, L. X. Zhou, Z. J. Li, T. Liu, X. X. Xue, and K. Z. Xu, J. Chem. Phys. **125**, 154307 (2006).
[12] E. Weigold, S. T. Hood, I. E. McCarthy, and P. J. O. Teubner, Phys. Lett. **44A**, 531 (1973).
[13] S. Dey, I. McCarthy, P. Teubner, and E. Weigold, Phys. Rev. Lett. **34**, 782 (1975).
[14] N. Stolterfoht *et al.*, Phys. Rev. Lett. **87**, 023201 (2001).
[15] A. B. Voitkiv, B. Najjari, D. Fischer, A. N. Artemyev, and A. Surzhykov, Phys. Rev. Lett. **106**, 233202 (2011).
[16] D. Rolles *et al.*, Nature (London) **437**, 711 (2005).
[17] S. E. Canton, E. Plesiat, J. D. Bozek, B. S. Rude, P. Decleva, and F. Martin, Proc. Natl. Acad. Sci. U.S.A. **108**, 7302 (2011).
[18] C. R. Stia, O. A. Fojn, P. F. Weck, J. Hanssen, and R. D. Rivarola, J. Phys. B **36**, L257 (2003).
[19] D. S. Milne-Brownlie, M. Foster, J. Gao, B. Lohmann, and D. H. Madison, Phys. Rev. Lett. **96**, 233201 (2006).
[20] E. M. Staicu-Casagrande *et al.*, J. Phys. B **41**, 025204 (2008).
[21] Z. N. Ozer, H. Chaluvadi, M. Ulu, M. Dogan, B. Aktas, and D. Madison, Phys. Rev. A **87**, 042704 (2013).
[22] J. P. D. Cook and C. E. Brion, Chem. Phys. **69**, 339 (1982).
[23] J. E. Pollard, J. Chem. Phys. **77**, 34 (1982).
[24] X. L. Han, V. Pozdin, C. Haridas, and P. Misra, J. Inf. Comput. Sci. **4**, 525 (2007).
[25] Z. J. Li, X. Chen, X. Shan, X. Xue, T. Liu, and K. Xu, Chem. Phys. Lett. **457**, 45 (2008).
[26] Z. J. Li, X. Shan, X.-F. Yang, K.-Z. Xu, and X.-J. Chen, J. Phys. Chem. A **112**, 942 (2008).
[27] V. G. Levin, V. G. Neudatchin, A. V. Pavlitchenkov, and Yu. F. Smirnov, J. Chem. Phys. **63**, 1541 (1975).
[28] J. N. Murrell and K. S. Sorbie, J. Chem. Soc., Faraday Trans. 2 **70**, 1552 (1974).
[29] M. J. Frisch *et al.*, in *GAUSSIAN 03, Revision B.04* (Gaussian, Inc., Pittsburgh, PA, 2003).
[30] Q. G. Tian, K. Wang, X. Shan, and X. Chen, Rev. Sci. Instrum. **82**, 033110 (2011).
[31] M. Yamazaki, H. Satoh, M. Ueda, D. B. Jones, Y. Asano, N. Watanabe, A. Czasch, O. Jagutzki, and M. Takahashi, Meas. Sci. Technol. **22**, 075602 (2011).